

# Shearlet, a Novel Operator Learning Model

Júlio Vargas   Bruno Jucá   Jairson Sami   Fábio Santos   Alexandre Evsukoff

National Laboratory of Scientific Computing (LNCC)  
Federal University of Rio de Janeiro (UFRJ)

May 15, 2026

Preprint: [arXiv:2604.25181](https://arxiv.org/abs/2604.25181)  
<https://arxiv.org/abs/2604.25181>

# Motivation: learning solution operators of parametric PDEs

## Problem statement

Given a parametric PDE

$$\mathcal{N}(u; a) = 0, \quad a \in \mathcal{A}, \quad u \in \mathcal{U},$$

learn the **solution operator**  $\mathcal{G}^\dagger : a \mapsto u$  from data, so that new instances of  $a$  can be mapped to  $u$  **without re-running** a classical solver.

## Why does this matter?

- Many-query problems: uncertainty quantification, design, inverse problems, control.
- Classical solvers are accurate but **expensive** when repeatedly evaluated.
- Neural operators trade offline training cost for **fast online inference**.

**The catch.** Real PDE solutions often exhibit:

- Anisotropic structures aligned with characteristics or material directions.
- Sharp gradients, fronts, and **shocks**.
- Multi-scale interactions.

# Neural operators in a nutshell

**Goal.** Approximate  $\mathcal{G}^\dagger$  between function spaces, in a discretization-invariant way.

A typical neural-operator layer acts on a hidden function  $v_t(x)$  as

$$v_{t+1}(x) = \sigma\left(W v_t(x) + [\mathcal{K}(a) v_t](x)\right),$$

combining a local linear map  $W$  with a non-local integral operator

$$[\mathcal{K}(a) v](x) = \int_D \kappa(x, y; a) v(y) dy.$$

**Design question:** how do we parameterise / compute  $\mathcal{K}$  efficiently?

- Graph kernels (GNO): flexible but costly.
- Low-rank kernels (LNO): efficient but global.
- Spectral parameterisation  $\Rightarrow$  FNO and its descendants.

# Fourier Neural Operator (FNO)

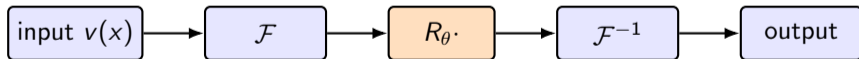
**Key idea.** Parameterise the integral kernel *in the spectral domain*: convolution becomes pointwise multiplication.

$$(\mathcal{K} v)(x) = \mathcal{F}^{-1}\left(R_\theta \cdot \mathcal{F}(v)\right)(x),$$

where  $\mathcal{F}$  is the Fourier transform and  $R_\theta$  is a learnable, frequency-truncated multiplier.

## Strengths

Fast (via FFT), mesh-agnostic, strong on smooth and periodic problems.



# Where FNO struggles

The Fourier basis  $\{e^{i\langle k,x \rangle}\}$  is:

- **Global**: every basis function is supported everywhere.
- **Isotropic**: no preferred direction.
- **Smooth**: poor at representing discontinuities (Gibbs phenomenon).

**Consequence.** For PDEs with

- **anisotropic** structure (e.g. strongly advective transport),
- **shocks and curved fronts** (conservation laws),
- **sharp interfaces** (multi-phase flows, multi-scale media),

FNO requires many modes and still smears out fine localized features.

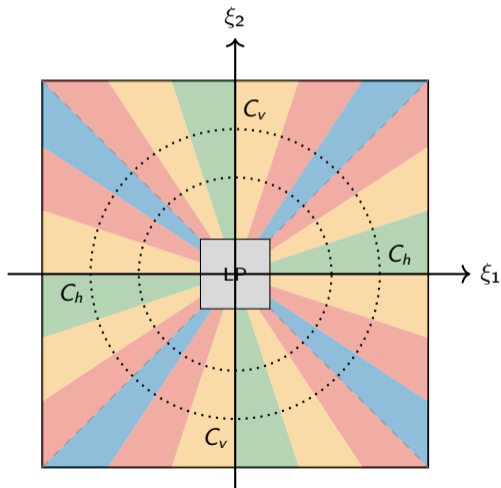
## What we want

A spectral representation that is **directional**, **multiscale**, and **spatially localized**.

⇒ **Shearlets**.

# Background — Shearlets: the intuition

*Cartoon-like* signals (images, PDE solutions): piecewise smooth with discontinuities along curves. We want a representation that is multiscale, directional, and spatially localised.



## Frequency-plane tiling.

- Two cones —  $C_h$  (horizontal) and  $C_v$  (vertical) — plus a central low-pass square.
- Each cone is split into **dyadic radial shells** indexed by scale  $j$ .
- Each shell is partitioned into **angular wedges** indexed by shear  $k$ .
- Finer scales  $\Rightarrow$  more wedges  $\Rightarrow$  better directional resolution.

## Three group operations:

- $A_a$  parabolic scaling
- $S_s$  shearing (orientation)
- $T_t$  translation (locality)

## Optimal sparse approximation (Guo & Labate)

For the class  $\mathcal{E}^2(\mathbb{R}^2)$  of *cartoon-like* functions (piecewise  $C^2$  with  $C^2$  edges), the best  $N$ -term shearlet approximation  $f_N$  satisfies

$$\|f - f_N\|_2^2 \lesssim N^{-2} (\log N)^3,$$

which is **optimal up to a log factor**, better than Fourier or wavelets.

### Three crucial properties:

- **Directional selectivity**: shear parameter resolves orientation, ideal for fronts and anisotropy.
- **Parabolic scaling**  $a \times \sqrt{a}$ : matches the geometry of curvilinear singularities.
- **Spatial localisation**: unlike Fourier atoms, each shearlet is concentrated around  $t$ .

These are exactly the features needed for shock-dominated PDE solutions.

# Background — Shearlets vs. Fourier vs. Wavelets

Property	Fourier	Wavelets	Shearlets
Spatial localisation	No	Yes	Yes
Multiscale	No	Yes	Yes
Directional selectivity	No	Limited	Yes
Anisotropic atoms	No	No	Yes
Sparse approx. of curved edges	$N^{-1/2}$	$N^{-1}$	$N^{-2}(\log N)^3$
Fast transform available	FFT	FWT	Fast Shearlet Transform

## Take-away

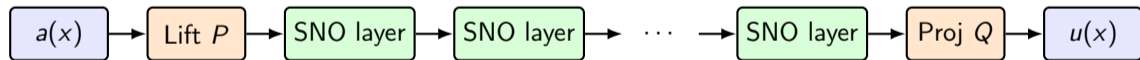
Shearlets keep the spectral-style efficiency that makes FNO attractive, while supplying the **geometric inductive bias** that Fourier lacks.

# Shearlet Neural Operator (SNO) — architecture

**Idea.** Replace the Fourier transform in the spectral layer of FNO with the discrete shearlet transform SH.

A single SNO layer applied to a hidden representation  $v_t$ :

$$v_{t+1}(x) = \sigma\left(W v_t(x) + \text{SH}^{-1}(R_\theta \odot \text{SH}(v_t))(x)\right).$$



**Pipeline.** Lifting  $P \rightarrow$  stacked SNO layers  $\rightarrow$  projection  $Q$  to physical output.

# Benchmark suite — seven PDE families

We compare SNO against FNO on **seven 2D parametric problems** grouped by regime:

## Diffusion-dominated

- **Multi-orientation texture** — anisotropic diffusion of superposed oriented waves.

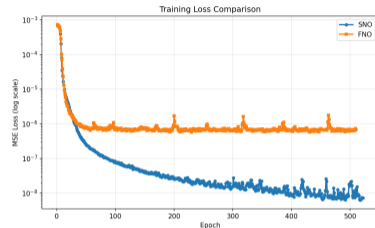
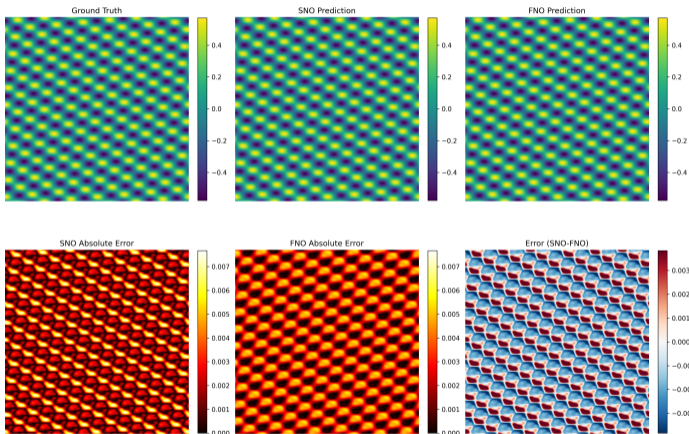
## Convection-dominated

- **Bent ridge advection** — parabolically curved front.
- **Anisotropic ridge advection** — extreme aspect-ratio jet ( $c_y/c_x = 120$ ).
- **Sheared Kelvin–Helmholtz stripes** — noisy oriented stripes.
- **Polygonal shock pattern** — 6-fold angular symmetry.

## Combined-effect (Burgers, low viscosity)

- **Multi-angle shocks** — two interacting shock fronts.
- **Spiral shock** — Archimedean spiral with continuously varying orientation.

# Results — Multi-orientation texture (diffusion)

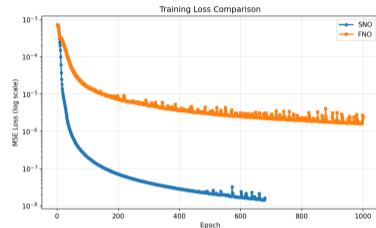
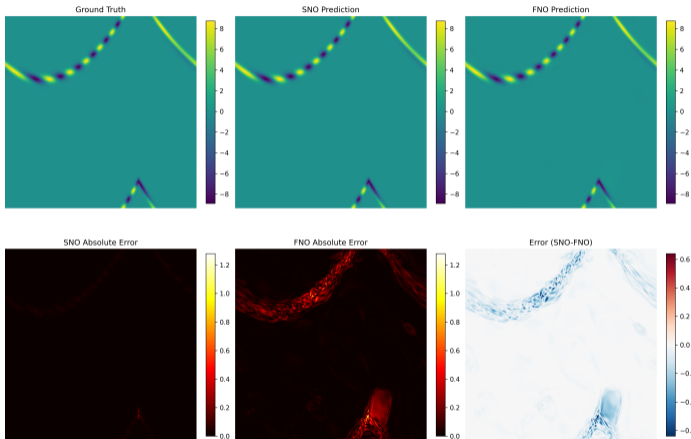


Training loss (MSE, log).

- FNO error visibly larger inside the oriented bands; SNO recovers them sharper.
- Both operators capture the multi-scale texture;  $L^2$  ratio  $\approx 0.97$  — near-tie at this resolution.
- FNO loss plateaus earlier; SNO converges faster in the early epochs.

Anisotropic diffusion of superposed oriented waves. ( $N=512$ ,  $T=150$ )

# Results — Bent ridge advection

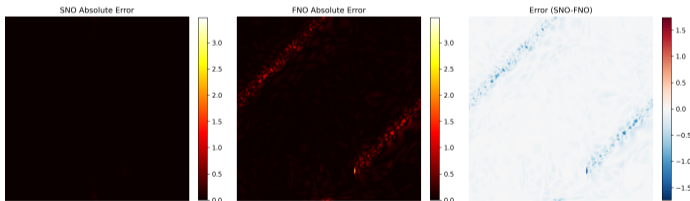
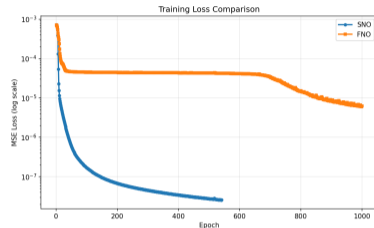
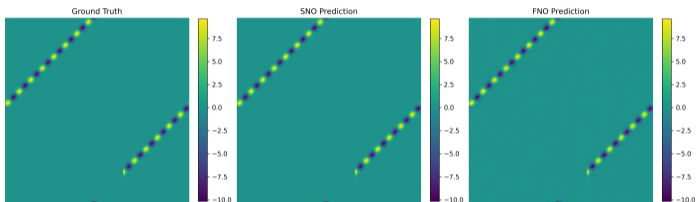


Training loss (MSE, log).

- SNO error near zero along the curved trajectory; FNO smears it over a wide tube.
- $L^2$  ratio (SNO/FNO)  $\approx 0.10$  — an order of magnitude better.
- Loss gap is roughly two orders of magnitude throughout training.

Curved front advected with  $(c_x, c_y) = (0.5, 5)$ . ( $N=512, T=150$ )

# Results — Anisotropic ridge advection (jet stream)

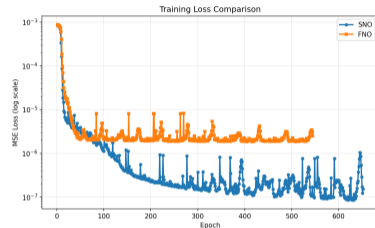
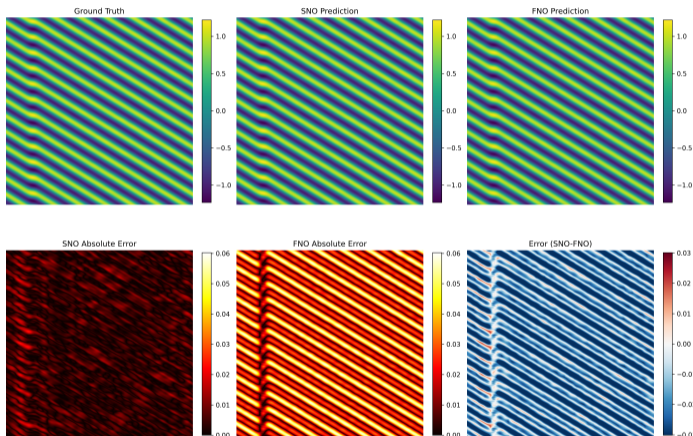


Training loss (MSE, log).

- Extreme directional bias: FNO's isotropic modes cannot align with the jet.
- SNO captures the oriented ridge essentially exactly.
- **Largest gap of the suite:  $L^2$  ratio  $\approx 0.06$  ( $\sim 16\times$ ); SSIM 0.9999 vs. 0.958.**

Aspect-ratio 120 transport,  $(c_x, c_y) = (0.05, 6.0)$ . ( $N=512, T=150$ )

# Results — Sheared Kelvin–Helmholtz stripes

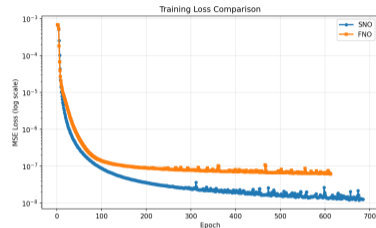
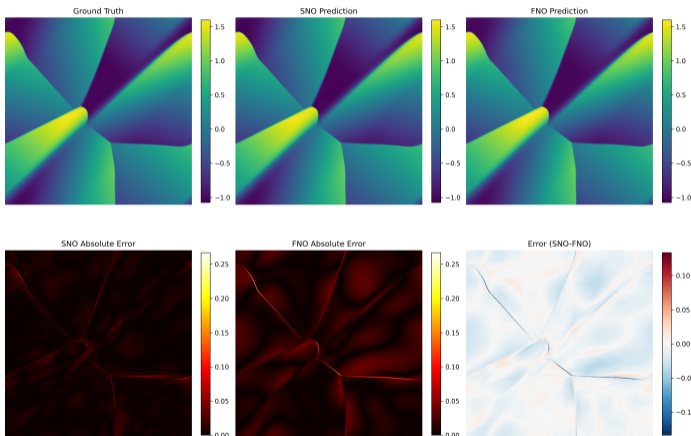


Training loss (MSE, log).

- Noise stresses both operators, but SNO retains stripe orientation and contrast.
- FNO loses stripe sharpness; SSIM drops to 0.968 vs. 0.999 for SNO.
- $L^2$  ratio  $\approx 0.18$  — consistent 5–6 $\times$  improvement.

Sheared stripes with additive Gaussian noise. ( $N=512$ ,  $T=100$ )

# Results — Polygonal shock pattern

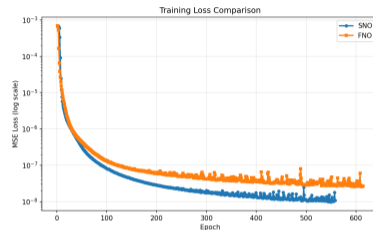
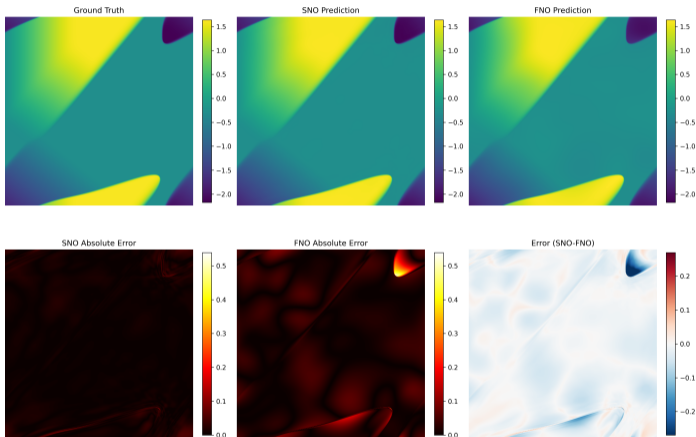


Training loss (MSE, log).

- FNO rounds the polygon's corners; SNO preserves the sharp vertices.
- Error concentrates on the discrete symmetry axes.
- $L^2$  ratio  $\approx 0.43$  — gap narrows because structure aligns partly with grid.

Hexagonal shock with 6-fold symmetry. ( $N=512$ ,  $T=220$ )

# Results — Multi-angle shocks (Burgers)

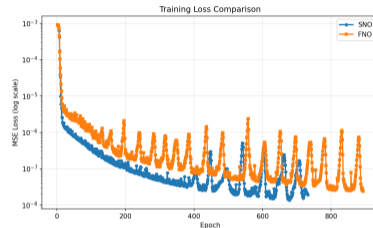
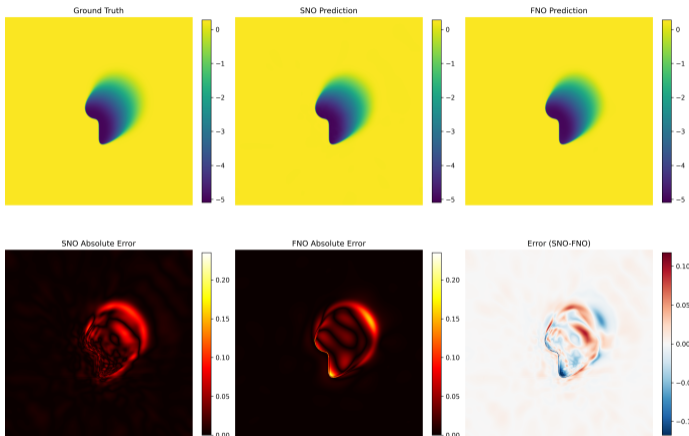


Training loss (MSE, log).

- SNO is visually indistinguishable from ground truth across the domain.
- FNO blurs both fronts and introduces oscillations near intersections.

Two interacting shock fronts at  $\arctan(0.8)$  and  $\arctan(-1.2)$ . ( $N=512$ ,  $T=220$ )

# Results — Spiral shock pattern (Burgers)



Training loss (MSE, log).

- Continuously rotating front: the hardest case for a finite shear discretisation.
- SNO still wins overall; FNO slightly better in smooth interior regions (red/blue mix).
- $L^2$  ratio  $\approx 0.99$  — essentially tied; limiting case for SNO's bias.

Archimedean spiral with continuously varying orientation. ( $N=512$ ,  $T=100$ )

# Quantitative comparison — all benchmarks ( $N=512$ )

Table: Performance Comparison between SNO and FNO Models for  $N = 512$

Dataset	SNO L2	FNO L2	Ratio	SNO MSE	FNO MSE	SNO MAE	FNO MAE	SNO SSIM	FNO SSIM
anisotropic ridge advect	$2.41 \times 10^{-6}$	$3.97 \times 10^{-5}$	0.0608	$3.36 \times 10^{-5}$	$9.08 \times 10^{-3}$	$2.11 \times 10^{-3}$	$4.60 \times 10^{-2}$	0.9999	0.9583
multi angle shocks	$3.93 \times 10^{-6}$	$1.48 \times 10^{-5}$	0.2650	$9.08 \times 10^{-5}$	$1.29 \times 10^{-3}$	$6.25 \times 10^{-3}$	$2.17 \times 10^{-2}$	0.9990	0.9942
bent ridge advect	$2.53 \times 10^{-6}$	$2.52 \times 10^{-5}$	0.1004	$3.69 \times 10^{-5}$	$3.67 \times 10^{-3}$	$2.43 \times 10^{-3}$	$2.24 \times 10^{-2}$	0.9999	0.9780
multi orientation texture	$4.09 \times 10^{-6}$	$4.21 \times 10^{-6}$	0.9699	$8.38 \times 10^{-6}$	$8.91 \times 10^{-6}$	$2.25 \times 10^{-3}$	$2.46 \times 10^{-3}$	0.9986	0.9988
spiral shock	$8.36 \times 10^{-6}$	$8.49 \times 10^{-6}$	0.9852	$2.16 \times 10^{-4}$	$2.22 \times 10^{-4}$	$5.84 \times 10^{-3}$	$4.42 \times 10^{-3}$	0.9939	0.9942
polygonal shock	$3.52 \times 10^{-6}$	$8.18 \times 10^{-6}$	0.4308	$4.10 \times 10^{-5}$	$2.21 \times 10^{-4}$	$4.19 \times 10^{-3}$	$1.04 \times 10^{-2}$	0.9987	0.9934
sheared kelvin helmoltz	$4.18 \times 10^{-6}$	$2.31 \times 10^{-5}$	0.1812	$3.21 \times 10^{-5}$	$9.77 \times 10^{-4}$	$4.44 \times 10^{-3}$	$2.65 \times 10^{-2}$	0.9989	0.9677

- Gap grows with anisotropy and shock complexity; spiral shock and multi-orientation texture are the limiting near-tie cases.

**What changed?** Only the **spectral basis** — from Fourier exponentials to shearlet atoms. Architecture, training, data, parameter budget were held fixed (SNO actually uses *fewer* parameters:  $\sim 12k$  vs.  $\sim 17k$  for FNO).

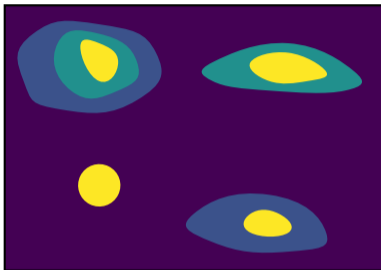
**Why such a large effect on hard regimes?**

- Fourier needs many modes to approximate localised, anisotropic features.
- Shearlets are near-optimal for cartoon-like functions  $\Rightarrow$  a small number of coefficients carries most of the information.
- The neural network only has to learn the **residual structure** once the basis already captures the geometry.

**Limitations.**

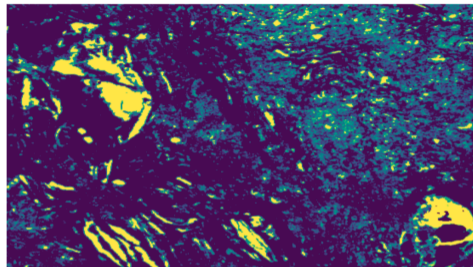
- Shearlet transforms have a higher constant cost than FFT.
- Cases with continuously varying orientation (spiral shock) erode the inductive-bias advantage.
- 3D extensions exist but are heavier to implement and train.

# Bridge — carbonate porosity slices *exhibit* cartoon-like structure



Synthetic cartoon  $f \in \mathcal{E}^2(\mathbb{R}^2)$ :

piecewise smooth on  $C^2$  regions; sharp jumps on a  $C^2$  curve.



Real porosity field ( $\mu$ CT):

Near-constant interiors, curved pore–solid interfaces.

## Why this matters

Similar structure: roughly constant interiors with sharp jumps along curved boundaries. The Guo–Labate  $N^{-2}(\log N)^3$  rate (slide 9) is optimal *exactly* for this signal class — a stronger fit than “anisotropic” alone.

# Application — Porosity prediction from dry rock samples

**Setting.** 3D porosity mapping of carbonate plug samples via micro-CT (COPPE/UFRJ × Petrobras).

## Classical pipeline (paired dry/wet $\mu$ CT)

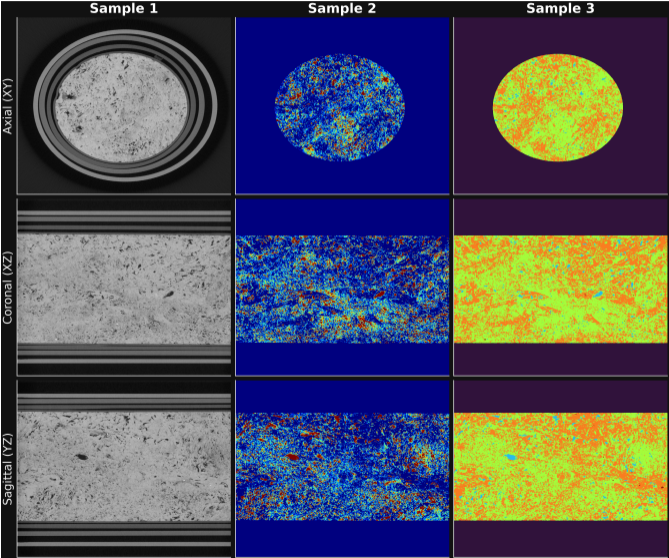
- Two scans of the *same* plug: **dry** and **saturated with 10% NaI at 2,500 psi**.
- Calibrated intensity difference gives voxel-wise porosity.
- Accurate but expensive: two scans, chemicals, high-pressure cel.

**Goal.** **Skip the wet scan** — predict the porosity map  $\phi(x) \in [0, 1]$  directly from the dry image alone, at *voxel scale*.

## Why is SNO a natural fit here?

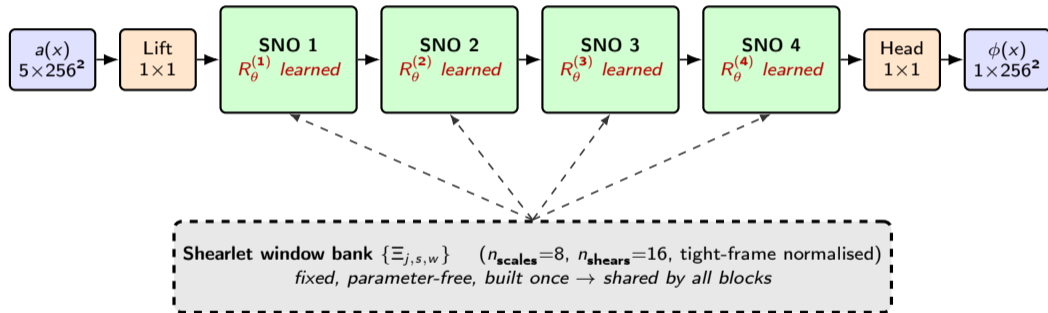
- Carbonate pore networks are **strongly anisotropic** (vugs, channels, oolitic shells, laminations).
- Pore-solid interfaces are **near-cartoon**: piecewise-smooth fields with curved  $C^2$  jump sets — the regime where shearlets give near-optimal sparse approximation.
- Dataset: **11 plugs**.

# Application — Porosity prediction from dry rock samples



# Spectral core — shared bank, per-block learned weights

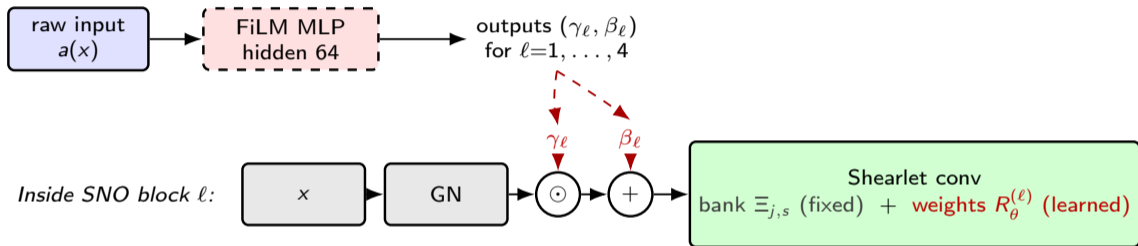
**Task.** Input:  $5 \times 256 \times 256$  (5 neighbouring dry slices). Output:  $1 \times 256 \times 256$  (central porosity slice).  
 $L=4$  spectral layers between a lift and a head.



**Inside each SNO block, all of these are learned, separately per block:** spectral mixing weights  $R_\theta^{(\ell)}$  acting on shearlet coefficients, sigmoid gates that combine the three mixing branches (spectral + depthwise  $3 \times 3$  + pointwise  $1 \times 1$ ), the depthwise/pointwise conv weights themselves, SE channel attention ( $r=4$ ), and the transformer-style FFN ( $4 \times$  expansion). Channel width  $W=16$  throughout. Per-sample GroupNorm ( $G=1$ ); long-range skip from lifted input to head.

# FiLM conditioning — how the *fixed* bank adapts per sample

**Feature-wise Linear Modulation.** A small MLP reads the raw input  $a$  and emits sample-specific scale/shift pairs  $\text{FiLM}(x; a) = \gamma(a) \odot x + \beta(a)$ , with  $(\gamma_\ell, \beta_\ell) \in \mathbb{R}^W \times \mathbb{R}^W$  for each of the  $L=4$  blocks ( $W=16$  values each).



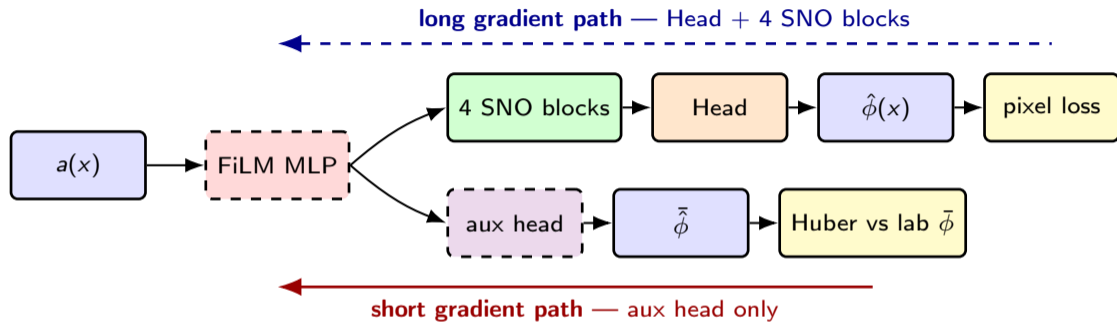
**Shared across samples** (set once during training):

- the shearlet bank  $\Xi_{j,s,w}$  (fixed mathematics, parameter-free);
- every learned weight:  $R_\theta^{(\ell)}$ , FiLM-MLP, sigmoid gates, depthwise/pointwise convs, SE, FFN.

**Sample-specific** (depend on *this*  $a(x)$ ):

- only the values  $(\gamma_\ell, \beta_\ell)$ ;
- $\gamma_\ell$  rescales each channel before the shearlet conv  $\Rightarrow$  the **fixed bank  $\Xi$  acts as an effectively different filter on each input**, without any weight changing.
- **Zero-init** ( $\gamma=1, \beta=0$  at step 0): training starts as if FiLM is absent.

# Auxiliary bulk-porosity head — a shortcut for global calibration



**What the aux head does.** A small MLP off the FiLM encoder predicts *one number* per sample — the bulk porosity:

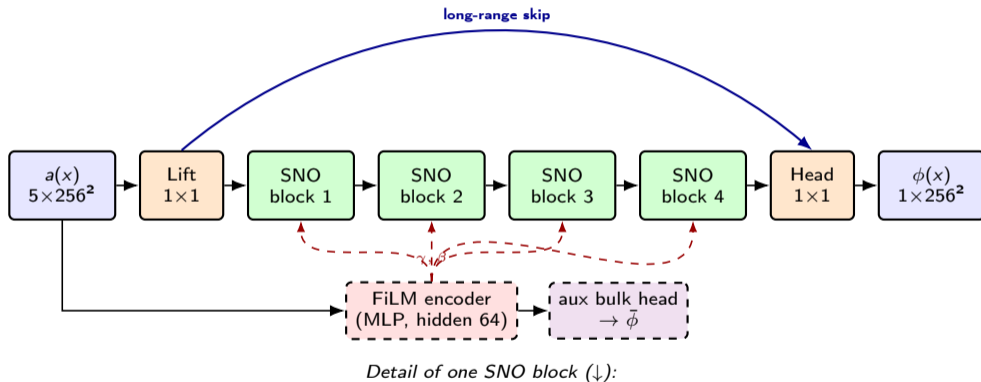
$$\tilde{\phi}(a) = \text{AuxHead}(\text{FiLM-MLP}(a)),$$

trained against the lab value with a Huber loss (weight 0.5).

**Why this matters.**

- Bulk porosity is a **sample-level** property; via pixel loss alone, calibration must back-propagate through 4 spectral blocks + head before reaching FiLM.
- Aux loss at the FiLM encoder gives a **one-step gradient path**  $\Rightarrow$  FiLM learns bulk *early*, so the spectral core can specialise on *spatial structure*.

# SNO for porosity — architecture diagram



# Training protocol — optimisation & LOOCV setup

## Optimisation

- AdamW,  $\beta = (0.9, 0.95)$
- $\eta = 10^{-3}$ ; weight decay  $10^{-4}$
- Batch size 32; gradient clip 2.0
- Up to 1000 epochs; early-stop patience 50 on `val_loss`
- GroupNorm-based per-sample input normalisation; no batch statistics

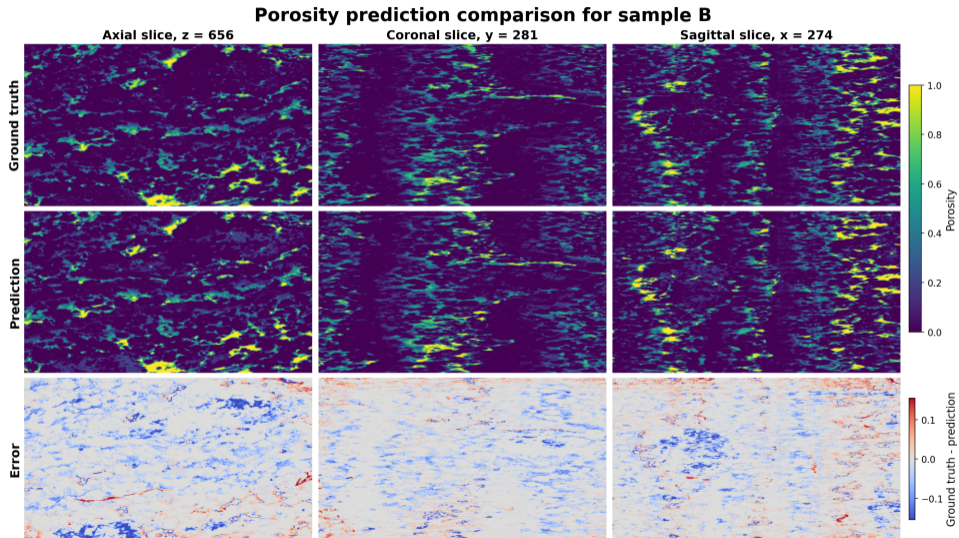
## LOOCV setup

- **11 sample codes**, one held out per fold ( $\times 11$  retrains)
- 90 / 10 train / val split within each fold
- **Sqrt-weighted** sample balancing (per-sample voxel count)
- DDP, multi-GPU; resumes from `last.ckpt`

## Reporting

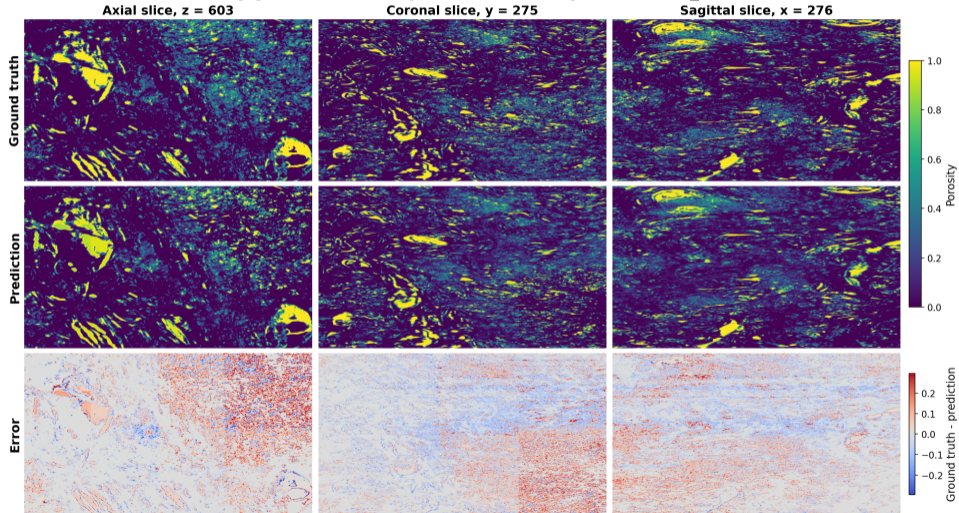
Test metrics are aggregated across the 11 held-out folds. Per-fold bulk porosities are then compared against laboratory measurements.

# Application results — visual prediction quality

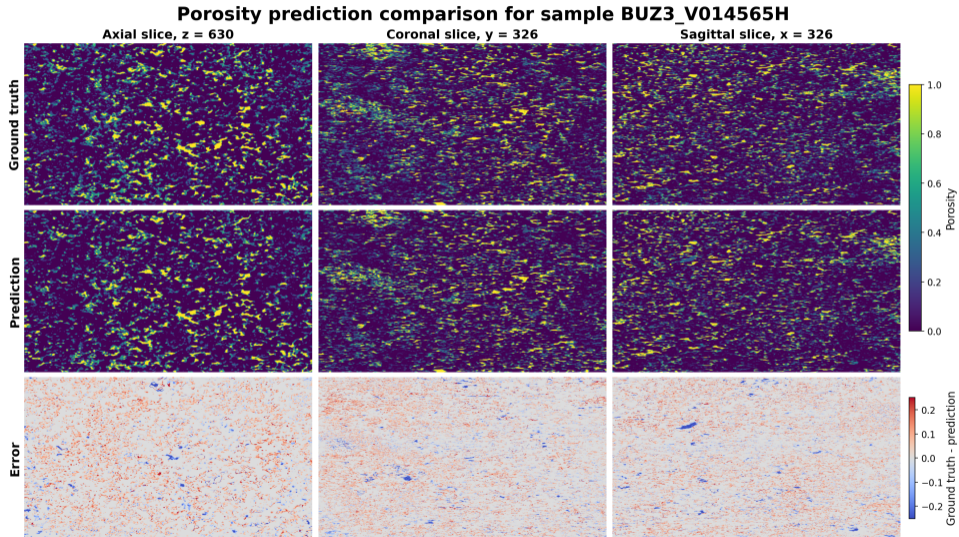


# Application results — visual prediction quality

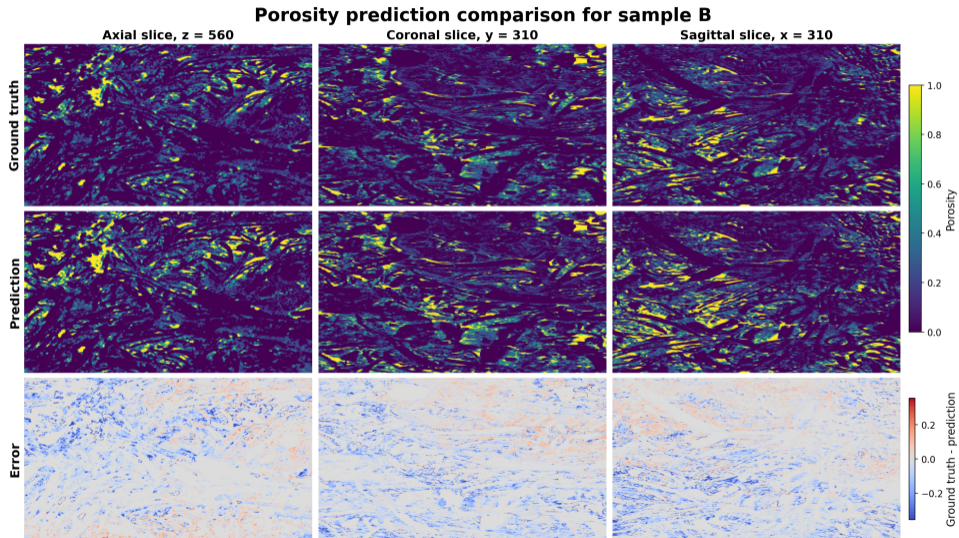
## Porosity prediction comparison for sample BUZ40D\_T013177H



# Application results — visual prediction quality

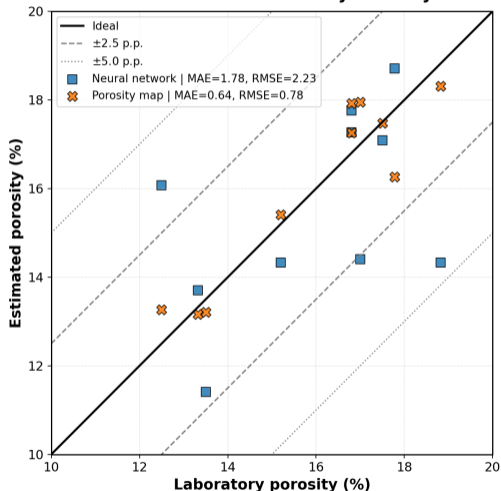


# Application results — visual prediction quality



# Application results — bulk porosity vs. classical CDF

Estimated vs. Laboratory Porosity



Predicted vs. lab bulk porosity, 11 plug crops, LOOCV.

Metric (p.p. unless noted)	Porosity map	SNO
MAE	0.64	1.78
RMSE	0.78	2.23
Bias	+0.18	-0.63
Median AE	0.51	0.96
Max AE	1.52	4.49
MAPE (%)	3.80	10.95
$R^2$	0.91	0.28
Within $\pm 1$ p.p. (%)	72.73	54.55
Within $\pm 2.5$ p.p. (%)	100.00	63.64
Within $\pm 5$ p.p. (%)	100.00	100.00

- SNO recovers **spatial structure** of pores per-slice (see prev. slide).
- Bulk calibration trails the porosity map method, which uses *both* dry+wet scans by construction.
- All SNO predictions remain within  $\pm 5$  p.p. of lab porosity — with the wet scan dropped.

## Contributions

- **SNO**: a neural operator built on the discrete shearlet transform — directional, multiscale, spatially-localised spectral layer.
- Consistent improvements over FNO on **anisotropic** and **shock-dominated** parametric PDEs across seven benchmark families, with *fewer* parameters.
- **Real-world case study**: 3D porosity mapping of carbonate rocks from dry-state micro-CT. SNO recovers pore geometry across 11 LOOCV folds; all bulk-porosity predictions within  $\pm 5$  p.p., *without* the saturated scan.

## Outlook

- 3D shearlets for compressible flow, seismic imaging, and full-volume porosity prediction.
- Hybrid Fourier / shearlet layers; physics-informed losses; adaptive band truncation.
- Tighten bulk-porosity calibration on the rock dataset (mass-conservation loss; larger / more diverse training cores).

## Preprint

F. P. dos Santos, J. de C. V. Fernandes, A. M. A. Côrtes. *Shearlet Neural Operators for Anisotropic-Shock-Dominated and Multi-scale Parametric PDEs*. arXiv:2604.25181 — [arxiv.org/abs/2604.25181](https://arxiv.org/abs/2604.25181)

Thank you — questions?